



Second harmonic conversions of surface-plasmon-polariton-enhanced optical fields in nonlinear optics polymer/Ag/glass structures

Atsushi Sugita, Suto Kaname, Kannta Mochizuki, and Kohei Kikuchi
Faculty of Engineering, Shizuoka University, Hamamatsu, Shizuoka 432-8561, Japan

Atsushi Ono
*Faculty of Engineering, Shizuoka University, Hamamatsu, Shizuoka 432-8561, Japan
 and Research Institute of Electronics, Shizuoka University, Hamamatsu, Shizuoka 432-8561, Japan*

Wataru Inami  and Yoshimasa Kawata
*Faculty of Engineering, Shizuoka University, Hamamatsu, Shizuoka 432-8561, Japan;
 Research Institute of Electronics, Shizuoka University, Hamamatsu, Shizuoka 432-8561, Japan;
 and A-STEP, Japan Science and Technology Agency, Chiyoda, Tokyo 102-0076, Japan*

 (Received 31 July 2019; revised manuscript received 8 January 2020; published 16 January 2020)

Optical fields enhanced by surface plasmon polaritons (SPPs) on metal-dielectric interfaces are useful for increasing several light-matter interactions, and application to nonlinear optics (NLO) is one of the most important uses of this type of structure. Most previous studies on this subject took advantage of the nonlinear susceptibilities of metal surfaces. However, the limited NLO light-matter interaction lengths prevented the transfer of the technologies to practical use. In the present paper, we tried to overcome this problem by growing NLO polymer thin films on metal surfaces. The NLO responses of the system were characterized by second-harmonic generation (SHG) spectroscopy. Our experimental results suggested that SPP-enhanced optical fields induced not only surface nonlinearities in Ag but also bulk nonlinearities in NLO polymer. There was an optimal polymer thickness for the SHG conversions, and a greater thickness did not always result in higher conversion. The maximum conversion efficiency was approximately 40 times higher than that of the nonpolymer-coated bare Ag surface. The growth and propagation of the SHG waves were addressed with a numerical approach combining the transfer matrix method and Green's function analysis. The SHG conversion efficiencies were determined by three factors, the SPP-field enhancement factor, the nonlinear light-matter interaction length, and the degree of interference between the forward- and backward-propagating SHG waves. The latter two factors predominantly determined the optimal SHG conversion efficiencies. The proposed strategy of hybridizing NLO polymers brings us closer to practical uses for nonlinear plasmonics.

DOI: [10.1103/PhysRevB.101.045303](https://doi.org/10.1103/PhysRevB.101.045303)

I. INTRODUCTION

A surface plasmon polariton (SPP) is an electromagnetic wave that propagates along a dielectric-metal interface [1–3]. The generation of SPPs results in significant enhancement of the electromagnetic fields in the immediate vicinity of the metal surfaces. Furthermore, the intensity of the enhanced field sharply decreases with increasing distance from the surface, and the SPPs are confined within nanometric spaces. The intense and confined optical fields due to SPPs are suitable for densely exciting materials in the vicinity of the metal surfaces and efficiently promote the light-matter interactions. The enhancements of Raman scattering cross sections [4–7], fluorescence quantum yield [8–10], and infrared absorptions [11,12] are some of the most important applications of optical fields enhanced by SPPs. These structures are also attractive as excitation light sources for nonlinear optics (NLO), in which multiple optical waves are mixed and converted to waves with sum or difference frequencies on the surfaces of the metals [13,14].

The NLO of SPPs were reported by H. J. Simon *et al.* as early as 1974 [15,16]. These researchers found intense second-harmonic generations (SHGs) from silver (Ag) films coupled with SPPs that were generated using prisms in Kretschmann configurations. These researchers also reported enhanced SHG through SPPs coupled with diffraction gratings [17,18]. There are a wide variety of NLO effects, depending on the number of photons and the frequencies and polarization states of the photons. The intense optical fields from SPPs are suitable for inducing the other NLO phenomena, such as sum-frequency generation [19,20], third-harmonic generation [21,22], and four-wave mixing [23,24]. There have been great advancements in nanofabrication technologies, and numerous unique plasmonic metal nanostructures have been proposed. Taking advantage of advanced plasmonic platforms, great efforts have been made toward not only converting the optical frequencies but also controlling the wave fronts of the frequency converted optical waves [25].

In the research and technology of NLO, it is important to determine the appropriate media in which NLO light-matter

interactions occur. Most previous research has been conducted using the surface nonlinearities of metals on which SPPs were created. Growing NLO active media on these metal surfaces was useful for further enhancing the efficiencies of the NLO wave mixing effects. LiNbO_3 [26], graphene [27,28], and organic dyes [29,30] are NLO media that have excellent track records for boosting NLO operations at SPP resonances. These materials are only a few of the NLO media reported [31]. It is crucial to explore the media that are of vital use in nonlinear plasmonics.

The present study was performed to explore the potential of NLO polymers as the media for boosting the nonlinear susceptibilities of the metal surfaces. The materials consist of guest chromophores and host polymeric materials [32–34]. The former play roles in nonlinear light-matter interactions, while the latter fold and fix the positions and orientations of the guests. Taking advantage of the flexible structural features of this material, nanometric thin films of NLO polymers can be easily fabricated on the surfaces of several types of materials, including metals. In addition, there have been many reports regarding the development of a wide variety of guest chromophores that have different resonant frequencies from the visible to near IR [35–37]. We can choose appropriate chromophores exhibiting the best NLO performances at arbitrarily targeted wavelengths.

In this study, *N*-ethyl-*N*-(2-hydroxyethyl)-4-(4-nitrophenylazo) aniline (DR1) and poly (methyl methacrylate) were chosen as the guest and the host, respectively. Combinations of DR1 and PMMA were among the most popular NLO polymers ever reported [38,39]. The applications of these polymers in optical frequency converters and electro-optic devices have been studied extensively. These polymers also exhibit a unique optical poling phenomenon, that is, the spontaneous polar ordering of the guest chromophores under simultaneous irradiation from fundamental and double-frequency light waves [40,41].

The research was performed by using a three-layer system consisting of an NLO polymer thin film, an Ag thin film, and a BK7 glass prism. Subsequently, the sample is referred to as the NLO polymer/Ag/BK7 structure. The SPPs were excited with an attenuated total reflection method in the Kretschmann geometry. The NLO properties of the model system were examined by the SHG method. We examined a reference system consisting of the bare PMMA/Ag/BK7 structure, in which the nonlinear susceptibility was attributed only to the Ag surface. We addressed the role of the bulk nonlinearities due to the NLO polymers in the vicinity of the dielectric-metal interfaces in comparison with the SHG behaviors of the reference system.

In addition, systems with different NLO polymer thicknesses were examined to explore the optimal polymer thickness for the highest SHG conversion efficiency. Furthermore, the growth and propagation of SHG waves in the vicinity of the Ag surface and inside the NLO polymer were numerically studied with a method that combined transfer matrix and Green's function analyses. We attempted to comprehensively understand the NLO light-matter interactions in the NLO polymer/Ag/BK7 structures by comparing the experimental and numerical results.

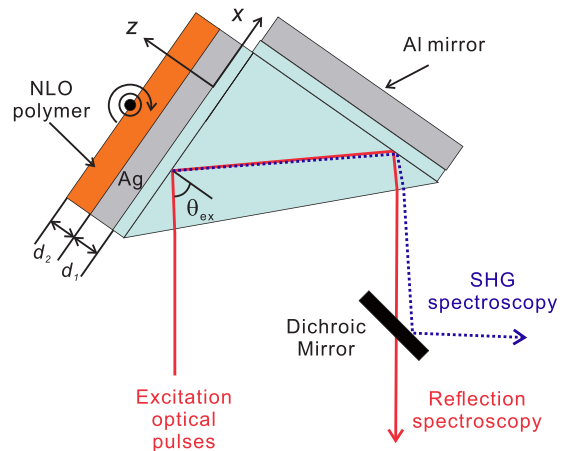


FIG. 1. Schematics of NLO polymer/Ag/BK7 structure and optical geometries for reflection and SHG spectroscopies.

II. EXPERIMENTAL

Figure 1 shows the schematics of the optical geometry for the reflectivity and SHG spectroscopies, along with the sample structure. The excitation light entered the samples through a Porro prism, or right-angle prism. The light retroreflected from the prism was detected for the reflectivity measurements and SHG signals. The angle of incidence of the excitation light was tuned by rotating the samples. The definition of the coordinates is shown in the same figure. Here, the plane of incidence is the xz plane, and the direction normal to the xy substrate surface is the z axis. The angle of incidence θ_{ex} is defined with respect to the z axis.

The samples were prepared as follows. First, Ag films were grown on BK7 glass substrates by a vacuum deposition method. Shots of Ag were evaporated with a resistive heater. The Ag film thickness was $d_1 = 43 \pm 2$ nm. Next, thin films of NLO polymer were grown on the Ag surfaces by a spin coating method. The guest DR1 and the host PMMA ($M_w = 1.2 \times 10^5$) were purchased from Sigma-Aldrich Co. The concentration of the guest in the NLO polymer was 10 wt %. The mixture of the guest and the host was dissolved in propionitrile. A drop of the solution was spanned on the Ag surface, and the solvent was dried. The thickness of the NLO polymer film was $d_2 = 0\text{--}80$ nm and it was controlled by changing the densities of the solvents in the solution. The thicknesses of the Ag and NLO polymer films were characterized with a surface profiler (Alpha-step D-500, KLA-tencor).

In general, NLO polymers do not exhibit second-order nonlinear susceptibilities in as-prepared conditions because the chromophores are randomly oriented to the host polymers and the structures of the materials are centrosymmetric. So-called poling procedures, procedures applying a DC electric field in these polymers, are conducted to align the chromophores to break the centrosymmetry and obtain second-order nonlinearities [38,39]. In a previous study, we found that the guest chromophores were aligned and spontaneously formed polar order after annealing [42,43]. Here, the polar ordering the guest chromophores was induced by nonelectrical poling techniques. Finally, the substrates were attached to the prisms. An index matching oil was implanted between

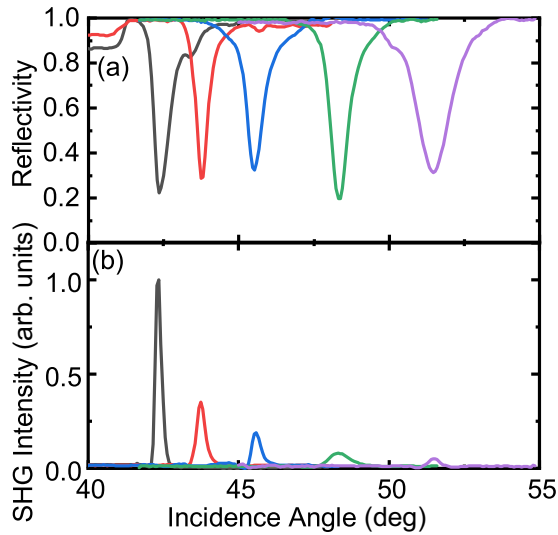


FIG. 2. (a) Reflectivity and (b) SHG signal intensities from PMMA/Ag/BK7 structure with the angle of incidence. The black, red, blue, green, and purple curves correspond to the data for the polymer thicknesses $d_2 = 0, 20, 40, 60,$ and 80 nm, respectively.

the prism and the substrate. An Al mirror was attached to the other surface of the prism to prevent transmission loss. The PMMA/Ag/BK7 structure, the reference system, was prepared using the same procedure.

The excitation light sources for the reflection and SHG spectroscopy were optical pulses (center wavelength: 780 nm, pulse width: 100 fs, and pulse energy: 2.6 nJ @ 75 MHz) from a mode-locked Ti: sapphire laser (Tsunami, Spectra-Physics, Inc.). The polarization direction of the excitation light was rotated with $\lambda/2$ wave plate. The angle of incidence θ_{ex} was controlled by rotating the samples by using a rotational stage equipped with a stepping motor. The reflection light was split into two by using a dichroic mirror that was designed to reflect fundamental light and transmit SHG light. The fundamental light was detected with an Si-photodiode (2032, Newport Co.) for the reflectivity measurements. The SHG light was detected with a photomultiplier tube (H9306-05, Hamamatsu Photonics K.K.) after removing the residual portion of the fundamental light with colored glass filters (390B, Sigma Koki Co.).

Both the reflection and SHG light were detected as a function of θ_{ex} . The retroreflected beam was displaced within the plane of incidence upon rotating the stage. The reflected and SHG light were collected with plano-convex lenses in front of the photodetectors. As d_2 was large, the retroreflected beam moved farther from the incident beam. The light signals were measurable in the regions $\theta_{\text{ex}} < 55^\circ$ in the present spectral apparatus.

Results

Figures 2(a) and 2(b) show the reflectivity and the SHG signal intensity as a function of θ_{ex} for the PMMA/Ag/BK7 structure for $d_2 = 0, 20, 40, 60,$ and 80 nm. The excitation light was p -polarized. The data at $d_2 = 0$ nm correspond to one for the nonpolymer-coated Ag/BK7 glass structure. The reflectivity spectrum exhibited a dip due to SPP resonance,

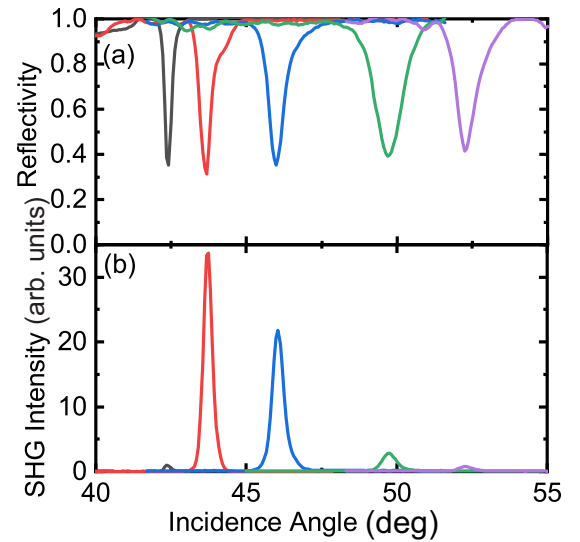


FIG. 3. (a) Reflectivity and (b) SHG signal intensities from NLO polymer/Ag/BK7 structure with angle of incidence. The black, red, blue, green, and purple curves correspond to the data for the polymer thicknesses $d_2 = 0, 20, 40, 60,$ and 80 nm, respectively.

independent of d_2 . The dip appeared at larger θ_{ex} for the structure with larger d_2 . Each structure had a peak in the SHG spectrum at the position of the dip. This observation indicates that the nonlinear light-matter interaction of the Ag surface was enhanced at the SPP resonance. The intensity of the SPP-enhanced SHG signals was lower as d_2 increased.

In a strict sense, the nonlinear wave mixing in the vicinity of the metal surfaces were caused not only by the surface responses but also by the bulk ones, which was expressed as $\Gamma \cdot \nabla(\vec{E} \cdot \vec{E})$ [44]. The term was related to the gradient of the electric field, and it gave significant contribution due to the variation of the field at the dielectric/metal interface. In practice, the bulk nonlinear susceptibility was dealt with as the additional term of the surface nonlinear susceptibility. In the later discussion, the nonlinear responses of the Ag will be addressed as the surfacelike responses and its nonlinear susceptibility will be referred to as the surfacelike nonlinear susceptibility.

The same measurements were conducted for the NLO polymer/Ag/BK7 structure. The reflectivity and SHG signals were plotted with θ_{ex} in Figs. 3(a) and 3(b), respectively. As in the case of the PMMA/Ag/BK7 structure, the reflectivity spectrum exhibited a dip due to the SPP resonance, independent of d_2 . The dip for the NLO polymer/Ag/BK7 structure occurred a slightly larger θ compared with that of the PMMA/Ag/BK7 structure. The difference between the positions of the dips of the two systems increased as d_2 increased because the refractive index of the NLO polymer was slightly higher than that of the bare PMMA and the SPP resonance condition was satisfied at a larger angle of incidence. A previous work reported that doping DR1 at 10 wt % resulted in an increase of approximately 2% in the refractive index of PMMA [45].

Intense SHG signals were obtained at the position of the dip in the NLO polymer/Ag/BK7 structure. The SPP resonance effect was helpful for increasing the NLO light-matter

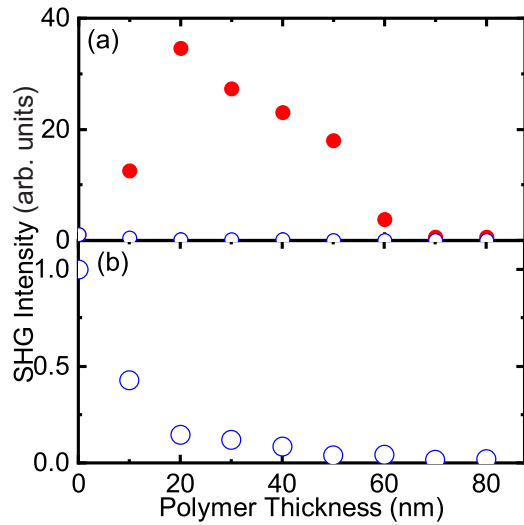


FIG. 4. (a) SHG intensity with polymer thickness for NLO polymer/Ag/BK7 (filled circles) and PMMA/Ag/BK7 structures (open circles). (b) Enlarged data for the PMMA/Ag/BK7 structure.

interactions in the structure. The SHG conversion efficiency was much higher than that of the PMMA/Ag/BK7 structure with the same d_2 . The SHG conversion process was attributed not only to the surface nonlinear susceptibility of Ag but also to the bulk of the NLO polymer.

The d_2 dependence of the SHG intensity for the NLO polymer/Ag/BK7 structure was essentially different from that for the PMMA/Ag/BK7 structure. Figure 4(a) shows the SHG intensity with d_2 for the two structures. The enlarged data for the PMMA/Ag/BK7 structure are shown in Fig. 4(b). In the PMMA/Ag/BK7 structure, the SHG signals monotonously decreased with d_2 increased. On the other hand, the SHG increased in the region $d_2 \leq 20$ nm, above which the SHG decreased for increasing d_2 in the NLO polymer/Ag/BK7 structure. The maximum SHG intensity at $d_2 \sim 20$ nm was approximately 35 times higher than that of $d_2 = 0$ nm, corresponding to the nonpolymer-coated Ag/BK7 structure. These results indicated that the SPP-enhanced optical fields induced nonlinear polarization inside the NLO polymer layer. The NLO polymer was useful for enhancing the NLO light-matter interactions at the SPP resonance. In addition, there was an optimal NLO polymer thickness for optimal SHG conversions.

The polarization behaviors of the SHG signals were studied to understand the NLO light-matter interactions from a geometric perspective. Figures 5(a) and 5(b) present the SHG intensities with the polarization angle of the excitation light for the NLO polymer/Ag/BK7 structures with $d_2 = 0$ and 40 nm. Here, the polarization angle γ_{ex} was defined with respect to the plane of incidence. The angle of incidence θ_{ex} was set to the position of the dip in Fig. 3(a) and the SHG signals were detected without resolving the polarization directions.

In both cases, the SHG intensities were the highest at $\gamma_{\text{ex}} = 0$ and 180° , while the intensities reached a minimum value of 0 at $\gamma_{\text{ex}} = 90$ and 270° . The data were reproduced

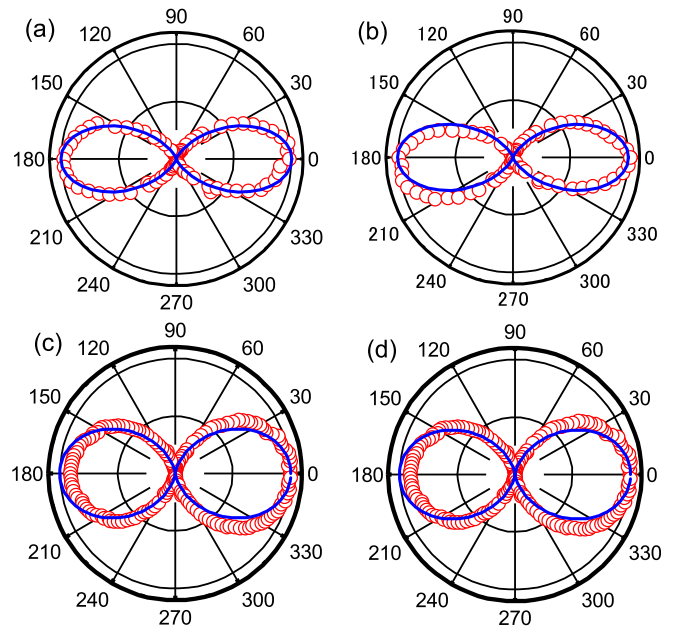


FIG. 5. (a) Excitation light polarization dependence of SHG signals for NLO polymer/Ag/BK7 structures with (a) $d_2 = 0$ and (b) 40 nm. Polarization states of SHG signals for the same sample with (c) $d_2 = 0$ and (d) 40 nm.

well with the $\cos^4 \gamma_{\text{ex}}$ -function, or the fourth power of the p -polarized field component $E_{\text{ex}} \cdot \cos \gamma_{\text{ex}}$. In general, SPP waves are coupled only with p -polarized light waves [46]. The γ_{ex} dependencies observed for the SHG intensities were consistent with expectations derived from the general rules.

Figures 5(c) and 5(d) present the polarization states of the SHG signals for the NLO polymer/Ag/BK7 structures with $d_2 = 0$ and 40 nm, respectively. Here, the polarization angle of the SHG waves γ_{SHG} was defined with respect to the plane of the incidence. The angle of incidence of the excitation lights with $\gamma_{\text{ex}} = 0^\circ$ was set at the peak of the dip for each sample. In both of the samples, the SHG intensities were the highest at $\gamma_{\text{SHG}} = 0$ and 180° , and the minimum was 0 at $\gamma_{\text{SHG}} = 90$ and 270° . The data were reproduced with the $\cos^2 \gamma_{\text{SHG}}$ function, and the SHG waves were p polarized.

The same measurements were performed for the systems with different d_2 . The γ_{ex} dependence of the SHG intensities and the γ_{SHG} -resolved SHG intensities were reproduced with the functions $\cos^4 \gamma_{\text{ex}}$ and $\cos^2 \gamma_{\text{SHG}}$, respectively, independent of d_2 . The nonlinear light-matter interactions at the SPP resonances were produced most efficiently by the p -polarized excitation lights, and the SHG waves were p polarized, independent of the thickness of the NLO polymer layer.

The second-order nonlinear susceptibilities were sensitive to the structure of the materials, and the forms of the tensor components were specific to the point symmetry of the material structures. The nonlinear light-matter interactions were attributed only to the surfacelike nonlinearities of Ag for the PMMA/Ag/BK7 structure. The geometry of the metal surface was regarded as $C_{\infty v}$ point symmetry, and there are three nonzero tensor components, $\chi_{\text{surf},zzz}^{(2)}$, $\chi_{\text{surf},zxx}^{(2)} = \chi_{\text{surf},zyy}^{(2)}$ and $\chi_{\text{surf},zxx}^{(2)} = \chi_{\text{surf},zyy}^{(2)}$ [44,47]. In the theoretical and experimental

results of previous studies, the $\chi_{\text{surf},zzz}^{(2)}$ component was much larger than the other components [30].

On the other hand, the SPP-enhanced fields oscillated within the plane of incidence and had x and z components. Hence, the z -polarized component of the SPP fields excited the nonlinear polarizations related to the $\chi_{\text{surf},zzz}^{(2)}$ component, which resulted in conversions into z -polarized SHG waves. The observations of p -polarized SHG waves in Fig. 5(c) were consistent with the expectations derived from the point symmetry of the system.

The nonlinear light-matter interactions were attributed to not only the surfacelike nonlinearities of Ag but also the bulk nonlinearities due to the NLO polymer in the NLO polymer/Ag/BK7 structure. The nonlinear susceptibilities of the NLO polymers were attributed to the polar ordering of the guest chromophores in the host polymers. In general, guest chromophores are oriented in a polar order along the direction normal to the substrate while randomly oriented within the plane of the surfaces. The polar ordering of the guest chromophores is regarded as $C_{\infty v}$ point symmetry, and there are three independent nonzero tensor components, $\chi_{\text{bulk},zzz}^{(2)}$, $\chi_{\text{bulk},zxx}^{(2)} = \chi_{\text{bulk},zxy}^{(2)}$ and $\chi_{\text{bulk},xzx}^{(2)} = \chi_{\text{bulk},yzy}^{(2)}$ [42,43].

The SPP-enhanced fields, which had x - and z -polarized components, were able to induce the nonlinear polarizations related to $\chi_{\text{bulk},zzz}^{(2)}$, $\chi_{\text{bulk},zxx}^{(2)}$, and $\chi_{\text{bulk},xzx}^{(2)}$. The polarizations due to the $\chi_{\text{bulk},zzz}^{(2)}$ and $\chi_{\text{bulk},zxx}^{(2)}$ components were converted into z -polarized SHG waves, while the polarizations due to the $\chi_{\text{bulk},xzx}^{(2)}$ component were converted into x -polarized SHG waves. Thus, the p -polarized SHG waves in Fig. 5(d) resulted from combining the x - and z -polarized SHG waves.

III. NUMERICAL

The SHG conversion procedures were numerically analyzed for the NLO polymer/Ag/BK7 and PMMA/Ag/BK7 structures with methods combining transfer matrix formalism and Green's function analyses. The details of the analysis are presented in Refs. [48–50]. First, the distributions of the electric field were calculated inside the systems with the transfer matrix formalism at the fundamental frequency ω . Second, the nonlinear frequency conversions were examined in the vicinity of the Ag surface and inside the NLO polymer layer. The rise of the SHG waves inside the NLO polymer layer was simulated with the Green's function method. Finally, the propagations of SHG waves were tracked inside the system with transfer matrix formalism.

Figure 6 shows the definitions of the coordinates of the four-layer model system. The schematics of the propagations of the optical fields are also shown in the same figure. Here, the layers $i = 0, 1, 2,$ and 3 correspond to the BK7 substrate, Ag layer, polymer layer, and atmosphere, respectively. The polymer layer consists of the NLO polymer in the NLO polymer/Ag/BK7 structure and the bare PMMA in the PMMA/Ag/BK7 structure. $n_i(\Omega)$ is the refractive index of the layer i at the frequency $\Omega (= \omega$ or $2\omega)$. The thicknesses of the Ag and the polymer layers are d_1 and d_2 , respectively. The z axis is normal to the layer, and the xz plane is the plane of incidence. The planes at $z_0 = 0$, $z_1 = d_1$, and $z_2 =$

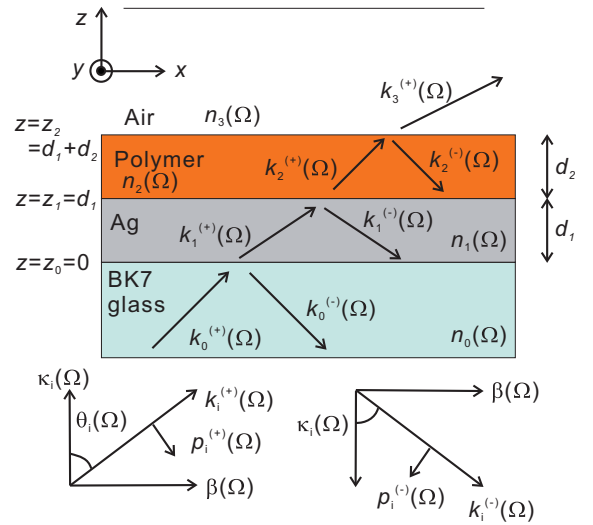


FIG. 6. Definitions of coordinates in four layer systems and propagation directions of forward- and backward-propagating light waves.

$d_1 + d_2$ correspond to the BK7/Ag, the Ag/polymer, and the polymer/air interfaces, respectively.

There are forward-propagating electric fields toward the $+z$ direction and backward-propagating fields toward the $-z$ direction in each layer. The wave vector of the optical field is defined as

$$\vec{\mathbf{k}}_i^{(\pm)}(\Omega) = \beta(\Omega) \cdot \hat{x} \pm \kappa_i(\Omega) \cdot \hat{z}, \quad (1)$$

where the plus and minus subscripts correspond to the forward- and backward-propagating waves, respectively. The absolute value of the wave vector is $k_i(\Omega) = |\vec{\mathbf{k}}_i^{(\pm)}(\Omega)| = \Omega \cdot n_i(\Omega)/c$. $\beta(\Omega)$ is the component of the wave vector parallel to the xy plane. Since the tangential component of the electric field is continuous across the surface, $\beta(\Omega)$ is common in all the layers. $\kappa_i(\Omega)$ is the z component of the wave vector in layer i and is given by $\kappa_i(\Omega) = \sqrt{k_i(\Omega)^2 - \beta^2}$. Here, the optical responses to the p -polarized light were examined. The polarization direction of the optical fields is expressed as

$$\vec{\tilde{p}}_i^{(\pm)}(\Omega) = \frac{1}{k_i(\Omega)} (-\beta(\Omega) \cdot \hat{z} \mp \kappa_i(\Omega)) \cdot \hat{x}. \quad (2)$$

Alternatively, $\vec{\tilde{p}}_i^{(\pm)}(\Omega)$ can be described as Eq. (3) by using the angle of refraction $\theta_i(\Omega)$ as

$$\vec{\tilde{p}}_i^{(\pm)}(\Omega) = -\sin \theta_i(\Omega) \cdot \hat{z} \mp \cos \theta_i(\Omega) \cdot \hat{x} \quad (3)$$

or

$$\begin{aligned} \vec{\tilde{p}}_i^{(\pm)}(\Omega) &= (p_{ix}^{(\pm)}(\Omega), p_{iy}^{(\pm)}(\Omega), p_{iz}^{(\pm)}(\Omega)) \\ &= (-\sin \theta_i(\Omega), 0, \mp \cos \theta_i(\Omega)). \end{aligned} \quad (4)$$

The forward- and backward-propagating electric fields in layer i can be written as

$$E_i^{(\pm)}(\Omega, \vec{r}) = \vec{\tilde{E}}_i^{\pm} \cdot \exp[i(\beta \cdot x \pm \kappa_i \cdot z)]. \quad (5)$$

Here, a two-component vector is defined as

$$\vec{\tilde{E}}_i(\Omega, z) = \begin{bmatrix} \vec{\tilde{E}}_i^{(+)} \cdot \exp(ik_i z) \\ \vec{\tilde{E}}_i^{(-)} \cdot \exp(-ik_i z) \end{bmatrix}. \quad (6)$$

At the i - $i + 1$ interface, the electric fields $\vec{E}_{i+1}(\Omega, z_i)$ and $\vec{E}_i(\Omega, z_i)$ are connected by Eq. (7):

$$\vec{E}_{i+1}(\Omega, z_i) = \mathbf{M}_{i+1,i} \vec{E}_i(\Omega, z_i). \quad (7)$$

The definition of the transfer matrix $\mathbf{M}_{i+1,i}(\Omega)$ is given by Eq. (8),

$$\mathbf{M}_{i+1,i}(\Omega) = \frac{1}{t_{i+1,i}(\Omega)} \begin{bmatrix} 1 & r_{i+1,i}(\Omega) \\ r_{i+1,i}(\Omega) & 1 \end{bmatrix}, \quad (8)$$

where $r_{i+1,i}(\Omega)$ and $t_{i+1,i}(\Omega)$ are the Fresnel reflection and transmission coefficients, respectively [51]. The phase and amplitude changes for the region $z_i \leq z_a \leq z_b \leq z_{i+1}$ in layer i are described by Eq. (9),

$$\vec{E}_i(\Omega, z_b) = \Phi_i(\Omega, z_b - z_a) \vec{E}_i(\Omega, z_a), \quad (9)$$

with

$$\Phi_i(z) = \begin{bmatrix} \exp(ik_i z) & 0 \\ 0 & \exp(-ik_i z) \end{bmatrix}.$$

We define the total 0–3 transfer matrix $\mathbf{U}(\Omega)$ for later discussion:

$$\begin{aligned} \mathbf{U}(\Omega) &= \begin{bmatrix} U_{11}(\Omega) & U_{12}(\Omega) \\ U_{21}(\Omega) & U_{22}(\Omega) \end{bmatrix} \\ &= \mathbf{M}_{32}(\Omega) \Phi_2(\Omega, z_2 - z_1) \mathbf{M}_{21}(\Omega) \Phi_1(\omega, z_1 - z_0) \\ &\quad \times \mathbf{M}_{10}(\omega). \end{aligned} \quad (10)$$

From here, the field distribution of the fundamental light frequency, ω , is mentioned. The optical field $\vec{E}_0(\omega, z_0)$ at the BK7/Ag interface is associated with the field $\vec{E}_3(\omega, z_2)$ at the polymer/air interface as

$$\begin{aligned} \vec{E}_3(\omega, z_2) &= \mathbf{M}_{32}(\omega) \Phi_2(\omega, z_2 - z_1) \mathbf{M}_{21}(\omega) \Phi_1(\omega, z_1 - z_0) \\ &\quad \times \vec{E}_0(\omega, z_0) \\ &= \mathbf{U}(\omega) \vec{E}_0(\omega, z_0). \end{aligned} \quad (11)$$

There are no backward-propagating optical fields in an atmosphere of air, and the condition $\vec{E}_3^{(-)}(\omega) = 0$ is

satisfied. Substituting the conditions into Eq. (11), the ratio $\vec{E}_1^{(-)}(\omega)/\vec{E}_1^{(+)}(\omega) = -U_{21}(\omega)/U_{22}(\omega)$ is obtained. Subsequently, the reflectivity and the electric field of the BK7 substrates are determined by Eqs. (12) and (13), respectively:

$$R(\omega) = \left| \frac{\vec{E}_0^{(-)}(\omega)}{\vec{E}_0^{(+)}(\omega)} \right|^2 = \left| -\frac{U_{21}(\omega)}{U_{22}(\omega)} \right|^2, \quad (12)$$

$$\vec{E}_0(z, \omega) = E_0^{(+)} \begin{bmatrix} 1 \\ -U_{21}/U_{22} \end{bmatrix}. \quad (13)$$

The SPP-enhanced electric field in the polymer layer is given by

$$\begin{aligned} \vec{E}_2(\omega, z) &= \begin{bmatrix} \sqrt{\eta_{\text{SP}}^{(+)}} \cdot \exp(i\phi_{\text{SP}}^{(+)}) \cdot \vec{E}_0^{(+)} \cdot \exp[i\kappa_2 z] \\ \sqrt{\eta_{\text{SP}}^{(-)}} \cdot \exp(i\phi_{\text{SP}}^{(-)}) \cdot \vec{E}_0^{(+)} \cdot \exp[-i\kappa_2 z] \end{bmatrix} \\ &= \Phi_2(\omega, z - d_1) \mathbf{M}_{21}(\omega) \Phi_1(\omega, d_1) \\ &\quad \times E_0^{(+)} \begin{bmatrix} 1 \\ -U_{21}(\omega)/U_{22}(\omega) \end{bmatrix}, \end{aligned} \quad (14)$$

where $\sqrt{\eta_{\text{SP}}^{(+)}} \cdot \exp(i\phi_{\text{SP}}^{(+)})$ and $\sqrt{\eta_{\text{SP}}^{(-)}} \cdot \exp(i\phi_{\text{SP}}^{(-)})$ are the complex SPP enhancement factors for the forward- and backward-propagating waves, respectively. Here, the electric field was taken on the polymer side of the interface.

Next, the nonlinear wave conversions in the vicinity of the Ag surface and in the polymer layer are discussed. The nonlinear optical responses are attributed to the surfacelike nonlinear susceptibilities of Ag and the bulk nonlinearities of the NLO polymer for the NLO polymer/Ag/BK7 structure. As mentioned above, the surfacelike-nonlinear susceptibility of the Ag was predominantly determined by $\chi_{\text{surf},zzz}^{(2)}$, while the bulk nonlinearities of the NLO polymer were expressed by the components $\chi_{\text{bulk},zzz}^{(2)}$, $\chi_{\text{bulk},zxx}^{(2)}$, and $\chi_{\text{bulk},xzx}^{(2)}$. On the other hand, the nonlinearity of the PMMA/Ag/BK7 structure was only due to $\chi_{\text{surf},zzz}^{(2)}$.

The forward- and backward-propagating fields create surfacelike nonlinear polarizations in the direction of the z axis at $z = z_1$, or on the Ag surface, as

$$P_{\text{surf}}^{(\pm)}(2\omega, z_1 = d_1) = \chi_{\text{surf},zzz}^{(2)} \cdot \{p_{2z}^{(\pm)}(\omega) \cdot \vec{E}_2^{(\pm)}(\omega, z_1) \cdot \exp[\pm i\kappa_2(\omega)z_1]\}^2. \quad (15)$$

Both of the nonlinear polarizations have the dependency on the term $\exp[2i\beta \cdot x]$ because of the propagation along the x axis. The term did not give any essential influence on the calculations of the SHG conversion. Hence, the contribution of the term is not expressed explicitly in Eq. (15).

It is conventional to choose the fundamental field just inside and place the polarization sheet just outside the metal layer [44]. Here, both of the fundamental fields and the polarization sheets were chosen just outside the Ag from the convenience for comparing the surfacelike nonlinear response of the Ag with that inside the NLO polymer layer. The surfacelike nonlinear susceptibility defined for the external field was smaller than that for the internal field by a factor of $\varepsilon_{\text{Ag}}^{-2}$ with ε_{Ag} , the dielectric constant of Ag.

The surfacelike polarizations radiate SHG electric fields $\vec{S}_{\text{surf}}(2\omega, z_1)$ as

$$\vec{S}_{\text{surf}}(2\omega, z_1) = \begin{bmatrix} S_{\text{surf}}^{(+)}(2\omega, z_1) \\ S_{\text{surf}}^{(-)}(2\omega, z_1) \end{bmatrix} = i \frac{(2\omega)^2}{2\varepsilon_0 c^2 \kappa_2(2\omega)} \begin{bmatrix} p_{2z}^{(+)} \cdot P_{\text{surf},z}^{(+)}(2\omega, z_1) \\ p_{2z}^{(-)} \cdot P_{\text{surf},z}^{(-)}(2\omega, z_1) \end{bmatrix}. \quad (16)$$

The forward- and backward-propagating SHG electric fields are expressed more explicitly as

$$\begin{aligned} S_{\text{surf}}^{(+)}(2\omega, z_1) &= i \frac{(2\omega)^2}{2\varepsilon_0 c^2 \kappa_2(2\omega)} \cdot \chi_{\text{surf,eff}}^{(2)} \cdot [\vec{E}_2^{(+)}(\omega)]^2 \cdot \exp[2i\kappa_2(\omega)z_1] \\ S_{\text{surf}}^{(-)}(2\omega, z_1) &= i \frac{(2\omega)^2}{2\varepsilon_0 c^2 \kappa_2(2\omega)} \cdot \chi_{\text{surf,eff}}^{(2)} \cdot [\vec{E}_2^{(-)}(\omega)]^2 \cdot \exp[-2i\kappa_2(\omega)z_1]. \end{aligned} \quad (17)$$

Here, $\chi_{\text{surf,eff}}^{(2)} = \chi_{\text{surf,zzz}}^{(2)} \cdot \sin^2 \theta_2(\omega) \cdot \sin \theta_2(2\omega)$ is the effective surfacelike nonlinear susceptibility of the Ag. The angle of refraction $\theta_2(2\omega)$ for the SHG waves is determined by the conservation of the wave vector along the x axis, that is, $\beta(2\omega) = 2\beta(\omega)$.

The cross term $\tilde{E}_2^{(+)} \cdot \tilde{E}_2^{(-)}$ also contributed to the SHG conversions. The SHG waves due to the term was bounded at the polymer/Ag interface and they could not be extracted outside of the structure [50]. The SHG conversion might also occurred at the Ag/SiO₂ interfaces. However, the electric fields did not gain the enhancements due to the SPP resonance at the interface, and they did not give any significant contributions to the SHG conversions. In the analysis, the SHG conversions at the Ag/SiO₂ interface was not taken into account.

The forward- and backward-propagating fundamental optical fields create nonlinear polarizations in the $a(=x, y, \text{ or } z)$ axis direction at the position z inside the NLO polymer layer as

$$P_{\text{bulk},a}^{(\pm)}(2\omega, z) = \sum_{b,c=x,y,z} \chi_{\text{bulk},abc}^{(2)} \cdot p_{2b}^{(\pm)}(\omega) \cdot \tilde{E}_2^{(\pm)}(\omega, z) \cdot \exp[\pm\kappa_2(\omega)z] p_{2c}^{(\pm)}(\omega) \cdot \tilde{E}_2^{(\pm)}(\omega, z) \cdot \exp[\pm\kappa_2z]. \quad (18)$$

The polarization at each point radiates the SHG electric fields. The SHG intensities increased with increasing propagation length. The superposed SHG electric field at position z is expressed as

$$\vec{S}_{\text{bulk}}(2\omega, z) = \begin{bmatrix} S_{\text{bulk}}^{(+)}(2\omega, z) \\ S_{\text{bulk}}^{(-)}(2\omega, z) \end{bmatrix} \quad (19)$$

with

$$S_{\text{bulk}}^{(+)}(2\omega, z) = i \frac{(2\omega)^2}{2\varepsilon_0 c^2 \kappa_2(2\omega)} \sum_{a=x,y,z} \int_{z_1}^z p_{2,a}^{(+)}(2\omega) \cdot P_{\text{bulk},a}^{(+)}(2\omega, z') \cdot \exp[i\kappa_2(2\omega)(z - z')] dz' \\ S_{\text{bulk}}^{(-)}(2\omega, z) = i \frac{(2\omega)^2}{2\varepsilon_0 c^2 \kappa_2(2\omega)} \sum_{a=x,y,z} \int_z^{z_2} p_{2,a}^{(-)}(2\omega) \cdot P_{\text{bulk},a}^{(-)}(2\omega, z') \cdot \exp[i\kappa_2(2\omega)(z - z')] dz'. \quad (20)$$

Integration was done from $z' = z_1$, or the polymer/Ag interface, to the point $z' = z$ for the forward-propagating wave, while integration was done from $z' = z$ to $z' = z_2$, or the air/polymer interface, for the backward-propagating wave. $S_{\text{bulk}}^{(+)}(2\omega, z)$ and $S_{\text{bulk}}^{(-)}(2\omega, z)$ are recast more explicitly as

$$S_{\text{bulk}}^{(+)}(2\omega, z) = i \frac{(2\omega)^2}{2\varepsilon_0 c^2 \kappa_2(2\omega)} \cdot \chi_{\text{bulk,eff}}^{(2)} \cdot [\tilde{E}_2^{(+)}(\omega)]^2 \frac{\exp[i\Delta\kappa_2 z] - \exp[i\Delta\kappa_2 z_1]}{\Delta\kappa_2} \cdot \exp[2i\kappa_2(\omega)z] \\ S_{\text{bulk}}^{(-)}(2\omega, z) = i \frac{(2\omega)^2}{2\varepsilon_0 c^2 \kappa_2(2\omega)} \cdot \chi_{\text{bulk,eff}}^{(2)} \cdot [\tilde{E}_2^{(-)}(\omega)]^2 \frac{\exp[-i\Delta\kappa_2 z_2] - \exp[-i\Delta\kappa_2 z]}{-\Delta\kappa_2} \cdot \exp[-2i\kappa_2(\omega)z]. \quad (21)$$

Here, $\Delta\kappa_2 = 2\kappa_2(\omega) - \kappa_2(2\omega)$ is the wave-number mismatch between the fundamental and SHG waves in layer 2. $\chi_{\text{bulk,eff}}^{(2)}$ is the effective nonlinear susceptibility and is given by

$$\chi_{\text{bulk,eff}}^{(2)} = \chi_{\text{bulk,zzz}}^{(2)} \cdot \sin^2 \theta_2(\omega) \cdot \sin \theta_2(2\omega) + \chi_{\text{bulk,zzx}}^{(2)} \cdot \cos^2 \theta_2(\omega) \cdot \sin \theta_2(2\omega) \\ + \chi_{\text{bulk,xxz}}^{(2)} \cdot \cos \theta_2(\omega) \cdot \sin \theta_2(\omega) \cdot \cos \theta_2(2\omega). \quad (22)$$

Finally, we discuss the propagations of the SHG waves inside the system. The solution of the wave equation with the nonlinear polarization term consists of the two fields, that is, the SHG fields driven by the nonlinear polarization and those free from them [50]. The driven SHG field existed only in the NLO polymer layer. The waves driven in the vicinity of the Ag surface and inside the NLO polymer correspond to Eqs. (16) and (19), respectively. On the other hand, the free fields $\vec{E}_i(2\omega, z)$ exist in all of the layers. The SHG fields inside the NLO polymer are expressed by the summation of the two SHG fields inside the NLO polymer layer.

The transfer of the SHG fields at the air/polymer interface is expressed as

$$\vec{E}_3(2\omega, z_2) = \mathbf{M}_{32}(2\omega)[\vec{E}_2(2\omega, z_2) + \vec{S}_{\text{surf}}(z_2) + \vec{S}_{\text{bulk}}(z_2)]. \quad (23)$$

Similarly, the transfer of the SHG field at the polymer/Ag interface is expressed as

$$\vec{E}_2(2\omega, z_1) + \vec{S}_{\text{bulk}}(z_1) + \vec{S}_{\text{surf}}(z_1) = \mathbf{M}_{21}(2\omega)\vec{E}_1(2\omega, z_1). \quad (24)$$

The growth and propagation of $\vec{S}_{\text{bulk}}(2\omega, z)$ inside the polymer layer is expressed by Eq. (19). The propagations of the $\vec{E}_2(2\omega, z_2)$ and $\vec{S}_{\text{surf}}(2\omega, z_2)$ are expressed by using $\Phi_2(2\omega, z_2 - z_1)$ as

$$\vec{E}_2(2\omega, z_2) = \Phi_2(2\omega, z_2 - z_1)\vec{E}_2(2\omega, z_1), \\ \vec{S}_{\text{surf}}(2\omega, z_2) = \Phi_2(2\omega, z_2 - z_1)\vec{S}_2(2\omega, z_1). \quad (25)$$

Combining Eqs. (23) and (24) with Eqs. (25), the SHG fields in the air atmosphere, $\vec{\mathbf{E}}_3(2\omega, z_2)$, are connected to those in the BK7 substrate, $\vec{\mathbf{E}}_0(2\omega, z_0)$, as

$$\vec{\mathbf{E}}_2(2\omega, z_3) = \mathbf{M}_{32}(2\omega)\Phi_2(2\omega, z_2 - z_1)\mathbf{M}_{21}(2\omega)\Phi_1(2\omega, z_1 - z_0)\mathbf{M}_{10}(2\omega)\vec{\mathbf{E}}_0(2\omega, z_0) + \mathbf{M}_{32}(2\omega)\vec{\mathbf{S}}(2\omega). \quad (26)$$

Here, the vector $\vec{\mathbf{S}}(2\omega)$ expresses the total superposition of the SHG waves radiated in the vicinity of the Ag surface and inside the NLO polymer layer. The vector is described using Eqs. (16) and (19) as

$$\vec{\mathbf{S}}(2\omega) = \begin{bmatrix} S^{(+)}(2\omega) \\ S^{(-)}(2\omega) \end{bmatrix} = \Phi_2(2\omega, z_2 - z_1)\vec{\mathbf{S}}_{\text{surf}}(2\omega, z_1) + \vec{\mathbf{S}}_{\text{bulk}}(2\omega, z_2) - \Phi_2(2\omega, z_2 - z_1)\vec{\mathbf{S}}_{\text{bulk}}(2\omega, z_1). \quad (27)$$

The vector is decomposed into two terms due to the Ag surface and NLO polymer as

$$\vec{\mathbf{S}}(2\omega) = \vec{\mathbf{S}}'_{\text{surf}}(2\omega) + \vec{\mathbf{S}}'_{\text{bulk}}(2\omega) \quad (28)$$

with

$$\begin{aligned} \vec{\mathbf{S}}'_{\text{surf}}(2\omega) &= \Phi_2(2\omega, z_2 - z_1)\vec{\mathbf{S}}_{\text{surf}}(2\omega, z_1), \\ \vec{\mathbf{S}}'_{\text{bulk}}(2\omega) &= \vec{\mathbf{S}}_{\text{bulk}}(2\omega, z_2) - \Phi_2(2\omega, z_2 - z_1)\vec{\mathbf{S}}_{\text{bulk}}(2\omega, z_1). \end{aligned} \quad (29)$$

The components $S'^{(+)}_{\text{surf}}(2\omega)$ for the forward- and $S'^{-}_{\text{surf}}(2\omega)$ for the backward-propagating waves are expressed as

$$\begin{aligned} S'^{(+)}_{\text{surf}}(2\omega) &= i \frac{(2\omega)^2}{\epsilon_0 c^2 \kappa_2(2\omega)} \cdot \chi_{\text{surf,eff}}^{(2)} \cdot [\tilde{E}_2^{(+)}(\omega)]^2 \exp[i\kappa_2(2\omega)(z_2 - z_1)] \cdot \exp[2i\kappa_2(\omega)z_1], \\ S'^{-}_{\text{surf}}(2\omega) &= i \frac{(2\omega)^2}{\epsilon_0 c^2 \kappa_2(2\omega)} \chi_{\text{surf,eff}}^{(2)} \cdot [\tilde{E}_2^{(-)}(\omega)]^2 \cdot \exp[-i\kappa_2(2\omega)(z_2 - z_1)] \cdot \exp[-2i\kappa_2(\omega)z_1]. \end{aligned} \quad (30)$$

The components $S'^{(+)}_{\text{bulk}}(2\omega)$ for the forward- and $S'^{-}_{\text{bulk}}(2\omega)$ for the backward-propagating waves are expressed as

$$\begin{aligned} S'^{(+)}_{\text{bulk}}(2\omega) &= i \frac{(2\omega)^2}{\epsilon_0 c^2 \kappa_2(2\omega)} \cdot \chi_{\text{surf,eff}}^{(2)} \cdot [\tilde{E}_2^{(+)}(\omega)]^2 \cdot \frac{\exp[i\Delta\kappa_2(z_2 - z_1)] - 1}{\Delta\kappa_2} \exp[i\kappa_2(2\omega)(z_2 - z_1)] \cdot \exp[2i\kappa_2(\omega)z_1], \\ S'^{-}_{\text{bulk}}(2\omega) &= i \frac{(2\omega)^2}{\epsilon_0 c^2 \kappa_2(2\omega)} \chi_{\text{surf,eff}}^{(2)} \cdot [\tilde{E}_2^{(-)}(\omega)]^2 \cdot \frac{\exp[-i\Delta\kappa_2(z_2 - z_1)] - 1}{-\Delta\kappa_2} \exp[-i\kappa_2(2\omega)(z_2 - z_1)] \cdot \exp[-2i\kappa_2(\omega)z_1]. \end{aligned} \quad (31)$$

When the polymer layer thickness $d_2 = z_2 - z_1$ is smaller than the phase-matching coherence length $1/\Delta\kappa_2$, that is, $z_2 - z_1 \ll 1/\Delta\kappa_2$, the phase-mismatching factor is approximated as $\exp[i\Delta\kappa_2(z_2 - z_1)]/\Delta\kappa_2 \approx \exp[-i\Delta\kappa_2(z_2 - z_1)]/(-\Delta\kappa_2) \approx i(z_2 - z_1) = id_2$. Equations (31) are approximated to

$$\begin{aligned} S'^{(+)}_{\text{bulk}}(2\omega) &= i \frac{(2\omega)^2}{\epsilon_0 c^2 \kappa_2(2\omega)} \cdot \chi_{\text{surf,eff}}^{(2)} \cdot [\tilde{E}_2^{(+)}(\omega)]^2 \cdot (z_2 - z_1) \exp[i\kappa_2(2\omega)(z_2 - z_1)] \cdot \exp[2i\kappa_2(\omega)z_1], \\ S'^{-}_{\text{bulk}}(2\omega) &= i \frac{(2\omega)^2}{\epsilon_0 c^2 \kappa_2(2\omega)} \chi_{\text{surf,eff}}^{(2)} \cdot [\tilde{E}_2^{(-)}(\omega)]^2 \cdot (z_2 - z_1) \exp[-i\kappa_2(2\omega)(z_2 - z_1)] \cdot \exp[-2i\kappa_2(\omega)z_1]. \end{aligned} \quad (32)$$

There are no forward-propagating waves in the BK7 substrate and no backward-propagating waves in air, that is, the condition $\tilde{E}_0^{(+)}(2\omega) = \tilde{E}_3^{(-)}(2\omega) = 0$ is satisfied. The backward-propagating SHG wave is determined by substituting the condition into Eq. (26):

$$\tilde{E}_0^{(-)}(2\omega) = -\frac{r_{32}(2\omega) \cdot S^{(+)}(2\omega) + S^{(-)}(2\omega)}{U_{21}(2\omega) \cdot t_{32}(2\omega)}. \quad (33)$$

The SHG signal intensity exiting into the BK7 layer is obtained by Eq. (34):

$$I_{\text{SHG}} = 2 \cdot n_0(2\omega)\epsilon_0 c \cdot |\tilde{E}_0^{(-)}(2\omega)|^2. \quad (34)$$

The numerical calculation showed that $\eta_{\text{SPP}}^{(+)}(\omega)$ was essentially equal to $\eta_{\text{SPP}}^{(-)}(\omega)$. Hence, the relationship $\eta_{\text{SPP}}^{(+)}(\omega) = \eta_{\text{SPP}}^{(-)}(\omega) = \eta_{\text{SPP}}(\omega)$ is assumed. The condition of total reflection is satisfied at the polymer/air interface at the SHG frequency. The Fresnel reflectivity is rewritten as $r_{32}(2\omega) = \exp(i\Delta\phi_{\text{ATR}})$. Equation (34) is rewritten by using these notations as

$$I_{\text{SHG}} = 2 \cdot n_0(2\omega)\epsilon_0 c \cdot \frac{\eta_{\text{SPP}}^2 \cdot |\tilde{E}_0^{(+)}|^4}{U_{22}(2\omega)t_{32}(2\omega)} \cdot (\chi_{\text{surf,eff}}^{(2)} + \chi_{\text{bulk,eff}}^{(2)}d_2)^2 |\exp[i(2\Delta\phi_{\text{SPP}} + 2\kappa_2(2\omega)d_2 + \Delta\phi_{\text{ATR}})] + 1|^2. \quad (35)$$

$\Delta\phi_{\text{SPP}} = \phi_{\text{SPP}}^{(+)} - \phi_{\text{SPP}}^{(-)} + 2\kappa_2(\omega)d_1$ is the phase difference between the forward- and backward-propagating

SPP-enhanced fields at $z = z_1$, or the polymer/Ag interface. $z_1 - z_0$ and $z_2 - z_1$ are replaced by d_1 and d_2 , respectively.

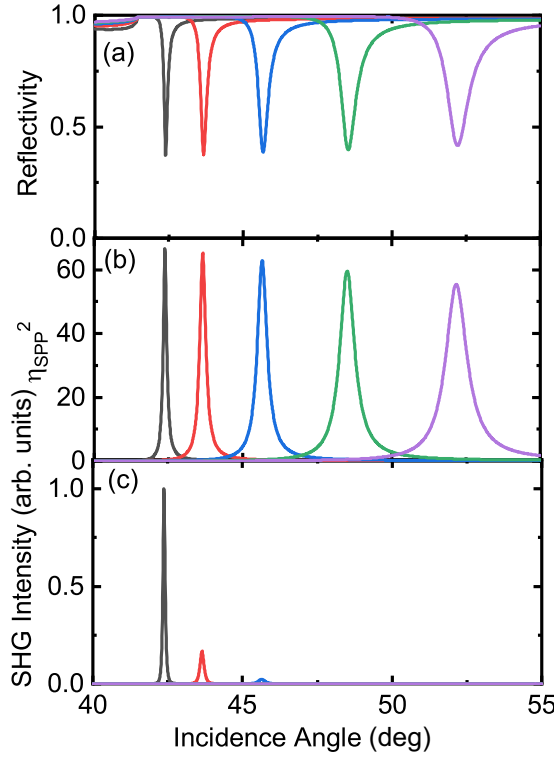


FIG. 7. (a) Reflectivity, (b) field enhancement, and (c) SHG signal numerically calculated with the transfer matrix method for PMMA/Ag/BK7 structure. The black, red, blue, green, and purple curves correspond to the data for polymer thicknesses $d_2 = 0, 20, 40, 60,$ and 80 nm, respectively.

Equation (35) consists of the products of the three terms. The first term, η_{SPP}^2 , is attributed to the field enhancements due to the SPP resonance. The second term, $(\chi_{\text{surf,eff}}^{(2)} + \chi_{\text{bulk,eff}}^{(2)} d_2)^2$, is related to the NLO light-matter interaction length inside the polymer layer. Since the polymer layer thickness was much smaller than the phase-matching coherence length, this term increases as a quadratic function of d_2 . The third term, $|\exp[i(2\Delta\phi_{\text{SPP}} + 2\kappa_2(2\omega)d_2 + \Delta\phi_{\text{ATR}}) + 1]|^2$, is related to the interference between the forward- and backward-propagating SHG waves. The degree of the interference depends on the three phase terms, that is, $\Delta\phi_{\text{SPP}}$, $2\kappa_2(2\omega)d_2$ and $\Delta\phi_{\text{ATR}}$. $\Delta\phi_{\text{SPP}}$ is the phase difference between the forward- and backward-propagating SPP-enhanced fields. $2\kappa_2(2\omega)d_2$ is caused by the propagation of the SHG waves inside the polymer layer. $\Delta\phi_{\text{ATR}}$ is the phase change of the forward-propagating SHG waves upon total reflection at the air/polymer interface.

IV. DISCUSSION

Figures 7(a) and 8(a) present the reflectivity with θ_{ex} , which were calculated numerically with Eq. (12), for the PMMA/Ag/BK7 and NLO polymer/Ag/BK7 structures, respectively. The calculations were performed for the systems for $d_2=0, 20, 40, 60,$ and 80 nm, and the polarization direction of the excitation light was p polarized. The refractive indexes of PMMA, BK7 glass and Ag were taken from references [52–54] in the calculation for the PMMA/Ag/BK7 structure.

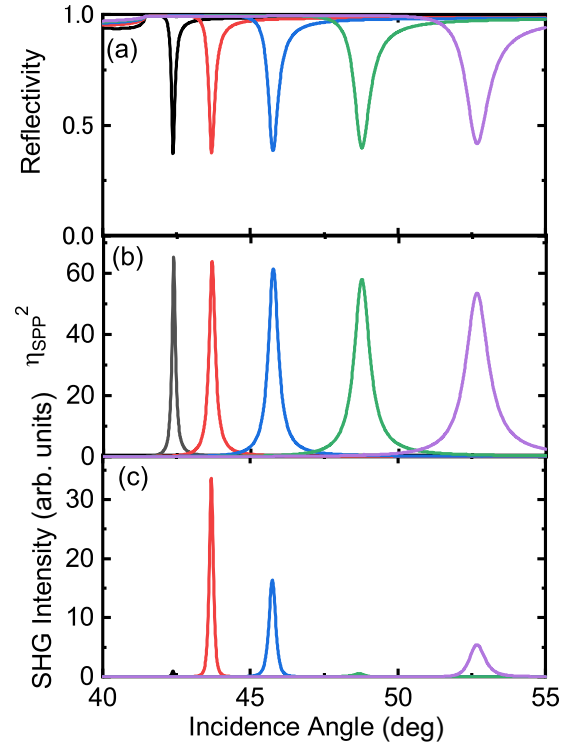


FIG. 8. (a) Reflectivity, (b) field enhancement, and (c) SHG signal numerically calculated with the transfer matrix method for NLO polymer/Ag/BK7 structure. The black, red, blue, green, and purple curves correspond to the data for polymer thicknesses $d_2 = 0, 20, 40, 60,$ and 80 nm, respectively.

The refractive index for the NLO polymer was assumed to be 2% above that of the bare PMMA in the calculation for the NLO polymer/Ag/BK7 structure. The dip structure was reproduced in the reflectivity spectrum calculated. Furthermore, the calculated position of the dip agreed with the experimental position.

The degree of the field enhancement η_{SPP}^2 was calculated with Eq. (14) and is presented in Fig. 7(b) for the PMMA/Ag/BK7 and Fig. 8(b) for the NLO polymer/Ag/BK7 structures. The present experiment was performed by using femtosecond optical pulses with a spectral width of $\Delta\lambda \sim 9$ nm. The calculated band width of η_{SPP}^2 was larger than $\Delta\lambda$. The calculations under the monochromatic conditions were available for analysis of the present experimental results. η_{SPP}^2 was weakly dependent on d_2 and slightly decreased at larger d_2 . η_{SPP}^2 at $d_2 = 80$ nm was 82% of the value at $d_2 = 0$ nm.

The SHG intensities were calculated with θ_{ex} for the PMMA/Ag/BK7 and NLO polymer/Ag/BK7 structures by using Eq. (35) and are shown in Figs. 7(c) and 8(c), respectively. In the calculation of the NLO polymer/Ag/BK7 structure, the parameters $\chi_{\text{bulk,zzz}}^{(2)}/\chi_{\text{surf,zzz}}^{(2)} = 4.5$ [nm], $\chi_{\text{bulk,zzx}}^{(2)}/\chi_{\text{bulk,zzz}}^{(2)} = 0.26$ and $\chi_{\text{bulk,xzx}}^{(2)}/\chi_{\text{bulk,zzz}}^{(2)} = 0.29$ were used. The surfacelike nonlinear susceptibility of Ag and the bulk of the NLO polymers are represented with different units. The former and the latter are $[\text{m}^2/\text{V}]$ and $[\text{m}/\text{V}]$, respectively. The ratios $\chi_{\text{bulk,zzx}}^{(2)}/\chi_{\text{bulk,zzz}}^{(2)}$ and $\chi_{\text{bulk,xzx}}^{(2)}/\chi_{\text{bulk,zzz}}^{(2)}$ were cited from the data of nonelectrically poled NLO

polymers on SiO₂ substrates from our previous study [42]. In the calculation of the PMMA/Ag/BK7 structure, the bulk nonlinear susceptibilities $\chi_{\text{bulk},zzz}^{(2)}$, $\chi_{\text{bulk},zxx}^{(2)}$ and $\chi_{\text{bulk},xzx}^{(2)}$ were set to zero, and only the surface susceptibility $\chi_{\text{surf},zzz}^{(2)}$ was considered.

In a precious sense, the nonlinear susceptibilities of the NLO polymer and Ag were complex. The wavelength dispersion of the phase in the susceptibilities had to be taken into account in the calculation for the NLO polymer/Ag/BK7 structure. In the present case, however, the absolute values of the susceptibilities were used for the calculations. It was because the SHG conversions were predominantly determined by the nonlinear polarizations due to the NLO polymers for the NLO polymer/Ag/BK7 structure, as will be seen later. The dispersion exerted the limited influences on them.

Equation (35) was derived under the condition that the polymer thickness was much smaller than the phase-matching coherence length, or $d_2 \ll 1/\Delta\kappa_2$. $1/\Delta\kappa_2$ was calculated by using $n_2(\omega) = 1.4847$ and $n_2(2\omega) = 1.5021$, or the refractive index of the polymer layer at the ω and 2ω -frequencies. This value was $1/\Delta\kappa_2 \sim 2.2 \mu\text{m}$ at $d_2 = 80 \text{ nm}$, the largest polymer thickness in the present study. Therefore, the condition $d_2 \ll 1/\Delta\kappa_2$ was satisfied and the use of Eq. (35) was valid.

The SHG spectra calculated reproduced several features of the experimental data of both structures. The monotonous decrease of the SHG intensity with d_2 was reproduced for the PMMA/Ag/BK7 structure. In the calculation for the NLO polymer/Ag/BK7 structure, the SHG intensities at $d_2 = 20$ and 40 nm were much higher than that at $d_2 = 0 \text{ nm}$, or the bare Ag surface, and decreased rather than increased at larger d_2 .

The calculation was performed for the structures with different d_2 to address the formation and propagation behaviors of the SHG waves in more detail. The SHG intensities at the SPP resonances were presented for the NLO polymer/Ag/BK7 and PMMA/Ag/BK7 structures in Figs. 9(a) and 9(b), respectively, along with the experimental data in Fig. 4. The SHG signals of the NLO polymer/Ag/BK7 structure were mostly converted by the bulk nonlinear susceptibility of the NLO polymer. The experimental data were reproduced well even without considering the surfacelike nonlinear susceptibility of Ag.

According to Eq. (35), the SHG conversion efficiencies are expressed as the product of three terms. The contributions of these terms are presented in Fig. 9(a). The first term, η_{SPP}^2 , is related to the degree of SPP-field enhancement. As mentioned above, this term slightly declined at larger d_2 . This factor does not play a predominant role in the d_2 dependence of the SHG conversion efficiencies. The second term, $(\chi_{\text{surf,eff}}^{(2)} + \chi_{\text{bulk,eff}}^{(2)} d_2)^2$, is related to the NLO light-matter interaction length. This term obeys the quadratic function of d_2 and monotonously increases as d_2 increases.

The third term, $|\exp[i(2\Delta\phi_{\text{SPP}} + 2\kappa_2(2\omega)d_2 + \Delta\phi_{\text{ATR}})] + 1|^2$, is given by the degree of interference between the forward- and backward-propagating SHG waves. The phase terms in the third were further decomposed into the three components $2\Delta\phi_{\text{SPP}}$, $2\kappa_2(2\omega)d_2$, and $\Delta\phi_{\text{ATR}}$. The term $2\Delta\phi_{\text{SPP}}$ relates to the phase shift imposed on the fundamental waves upon SPP resonance. The term $2\kappa_2(2\omega)d_2$ is caused by the

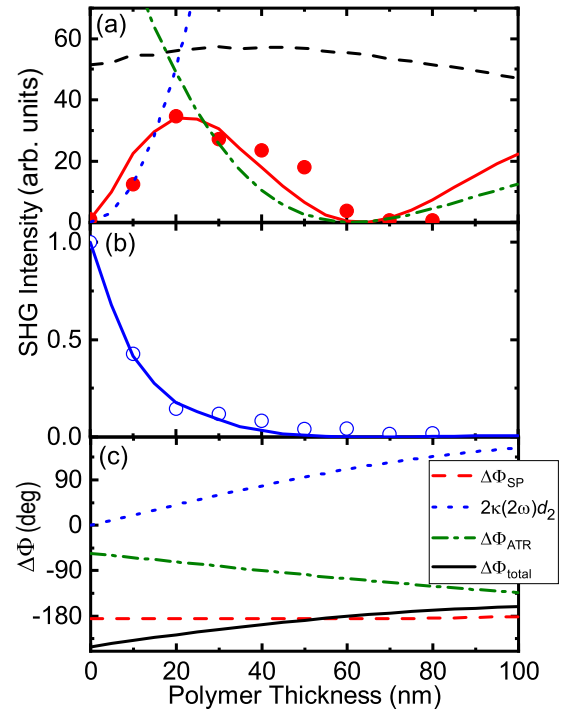


FIG. 9. (a) SHG intensity versus polymer film thickness for the NLO polymer/Ag/BK7 structure (red filled circles) along with the numerical data calculated with Eq. (33) (red solid curve). The constituent terms of η_{SPP}^2 (black dashed curve), $(\chi_{\text{surf,eff}}^{(2)} + \chi_{\text{bulk,eff}}^{(2)} d_2)^2$ (blue dotted curve), and $\exp[i(2\Delta\phi_{\text{SPP}} + 2\kappa_2(2\omega)d_2 + \Delta\phi_{\text{ATR}})] + 1|^2$ (green dash-dotted curve) are shown. (b) The same for the PMMA/Ag/BK7 structures. (c) The phase terms in Eq. (33). $\Delta\phi_{\text{total}}$ (black curve) is the summation of $\Delta\phi_{\text{SPP}}$ (red dashed curve), $2\kappa_2(2\omega)d_2$ (blue dotted curve), and $\Delta\phi_{\text{ATR}}$ (green dash-dotted curve).

propagation of the SHG waves inside the polymer layer and increased almost linearly with d_2 . The term $\Delta\phi_{\text{ATR}}$ is related to the change in the phase of the SHG waves due to attenuated total reflection (ATR) at the air/polymer interface. A pair of SHG waves interfered the most constructively at $\Delta\phi_{\text{total}} = 0^\circ$ and the most destructively at $\Delta\phi_{\text{total}} = \pm 180^\circ$.

The d_2 dependence of the total phase shift $\Delta\phi_{\text{total}}$ is shown in Fig. 9(c), along with the constituent components $2\Delta\phi_{\text{SPP}}$, $2\kappa_2(2\omega)d_2$, and $\Delta\phi_{\text{ATR}}$. The term $2\Delta\phi_{\text{SPP}}$ was almost independent of d_2 . The term $2\kappa_2(2\omega)d_2$ monotonously increased with d_2 , while $\Delta\phi_{\text{ATR}}$ decreased monotonously. The total phase difference $\Delta\phi_{\text{total}}$ was virtually determined by the terms $2\kappa_2(2\omega)d_2$ and $\Delta\phi_{\text{ATR}}$. The phase difference monotonously decreased with d_2 and crossed $\Delta\phi_{\text{total}} = -180^\circ$ at $d_2 \sim 60 \text{ nm}$. Therefore, the forward- and backward-propagating SHG waves interfered more destructively as the polymer thickness d_2 increased in the region $d_2 = 0 - 60 \text{ nm}$ and interfered more constructively in the region $d_2 > 60 \text{ nm}$ at larger d_2 .

In the calculation of the PMMA/Ag/BK7 structure, only the surfacelike nonlinear susceptibility was taken into account, and the nonlinear response was independent of d_2 . In addition, the term due to η_{SPP}^2 exhibited weak dependence on d_2 . The SHG conversion efficiency was predominantly determined by the term related to the interference between the

forward- and backward-propagating SHG waves. The good agreement between the experimental and numerical data met expectations. Equation (35) indicated that the SHG conversion efficiencies switched from decreasing to increasing at $d_2 = 60$ nm. However, $\Delta\phi_{\text{total}}$ was close to -180° in the region $60 < d_2 < 80$ nm, and the expected SHG intensities were much lower than that at $d_2 = 0$ nm. It is plausible that the SHG conversion efficiencies did not exhibit any significant increases in that region.

The SHG conversion efficiencies of the NLO polymer/Ag/BK7 structure were determined by not only the term related to the interference but also the term related to the NLO light-matter interaction length. As d_2 increased, the former monotonously decreased and the latter monotonously increased in the region $0 < d_2 < 60$ nm [Fig. 9(a)]. In the region $d_2 < 25$ nm, the former dominated the latter and vice versa at larger d_2 . The optimal condition of the SHG conversion efficiency was determined by the balance between the two factors. Both the forward- and backward-propagating SHG waves progressively increased inside the structures as d_2 increased, because of the longer light-matter interaction length in the NLO polymer layer. However, pairs of the SHG waves were superposed more destructively and were extracted less efficiently outside of prism at larger d_2 .

$\Delta\phi_{\text{total}}$ crossed -180° at $d_2 = 60$ nm. The forward- and backward-propagating SHG waves are expected to interfere more constructively and higher SHG signals are obtained at larger d_2 . In practice, the numerical data exhibited a buildup of the SHG signals in these regions. However, a buildup of the SHG signals was not clearly observed in the present experimental results.

The discrepancy between the experimental and numerical data was probably due to artifacts caused by the configurational restrictions of the present spectroscopic apparatus. Because of the angular dispersion in the prism, the rays of the SHG beams propagated off the axis of the retroreflected fundamental excitation light. The SHG beams were distanced from the beams of the excitation lights, and it is possible that the beams protruded from the effective areas of the reflection mirrors in the optical path or the focusing lens in front of the photodetector at larger θ_{ex} . The SHG waves were easier to measure in smaller ranges of θ_{ex} than the fundamental

waves and were not measured correctly in larger ranges of θ_{ex} .

V. CONCLUSIONS

The present paper reported the SHG behaviors of NLO polymer/Ag/BK7 structures at SPP resonances. Our experimental results proved that the growth of an NLO polymer on an Ag surface was suitable for enhancing the SHG conversion efficiencies of the system. The SHG conversion efficiencies were dependent on the NLO polymer thickness. The maximum SHG conversion efficiency was approximately 40 times higher than that of the nonpolymer-coated Ag/BK7 structure. The experiments were performed on a reference system consisting of the bare PMMA/Ag/BK7 structure. The SHG conversion efficiencies of the reference monotonously decreased as the polymer thickness increased.

The NLO light conversion procedures were numerically examined by using an approach combining the transfer matrix method with Green's function analysis. The experimental data were reproduced well by the numerical data. The SHG conversion efficiencies for the NLO polymer/Ag/BK7 structure were determined by the balance between the NLO light-matter interaction length inside the NLO polymer and the degree of the interference between the forward-propagating and backward-propagating SHG waves inside the NLO polymer layer. On the other hand, the conversion efficiencies of the reference system were predominantly determined by the latter factor. The present paper demonstrated that hybridizing plasmonic metal surfaces with NLO polymers was suitable for overcoming inadequate light-matter interaction lengths in existing nonlinear plasmonic systems.

ACKNOWLEDGMENTS

This work was supported by a Grant-in-Aid for Scientific Research (B) (Grant No. 26286059) from the Japan Society for the Promotion of Science (JSPS) and a Grant-in-Aid of a strategic-theme-focused type in the Adaptable and Seamless Technology Transfer Program through Target-driven R&D (Grant No. AS2720000X) from the Japan Science and Technology Agency.

-
- [1] A. A. Maradudin, in *Modern Plasmonics*, edited by A. A. Maradudin, J. R. Samples, and W. L. Barnes (Elsevier, Amsterdam, 2014), pp. 1–36.
 - [2] M. L. Brongersma and P. G. Kik, in *Surface Plasmon Nanophotonics*, edited by M. L. Brongersma and P. G. Kik (Springer, Dordrecht, 2007), pp. 1–9.
 - [3] D. Sarid and W. Challener, in *Modern Introduction to Surface Plasmonics—Theory, Mathematica Modeling and Applications* (Cambridge University Press, Cambridge, 2010), pp. 4–55.
 - [4] M. Fleischmann, P. J. Hendra, and A. McQuillan, *Chem. Phys. Lett.* **26**, 163 (1974).
 - [5] M. Moskovits, *Rev. Mod. Phys.* **57**, 783 (1985).
 - [6] K. Kneipp, H. Kneipp, I. Itzkan, R. R. Dasari, and M. S. Feld, *Chem. Rev.* **99**, 2957 (2008).
 - [7] L. Jensen, C. M. Aikens, and G. C. Schatz, *Chem. Soc. Rev.* **37**, 1061 (2008).
 - [8] K. H. Drexhage, *J. Lumin.* **1-2**, 693 (1970).
 - [9] J. Kummerlen, A. Leitner, H. Brunner, F. R. Aussenegg, and A. Wokaun, *Mol. Phys.* **80**, 1031 (1993).
 - [10] F. Tam, G. P. Goodrich, B. R. Johnson, and N. J. Halas, *Nano Lett.* **7**, 496 (2007).
 - [11] A. Hartstein, J. R. Kirtley, and J. C. Tsang, *Phys. Rev. Lett.* **45**, 201 (1980).
 - [12] M. Osawa and M. Ikeda, *J. Phys. Chem.* **95**, 9914 (1991).
 - [13] M. Kauranen and A. Zayats, *Nat. Photonics* **6**, 737 (2012).
 - [14] J. Butet, P. F. Brevet, and O. J. F. Martin, *ACS Nano* **9**, 10545 (2015).
 - [15] H. J. Simon, D. E. Mitchell, and J. G. Watson, *Phys. Rev. Lett.* **33**, 1531 (1974).

- [16] Z. Chen and H. J. Simon, *Opt. Lett.* **13**, 1008 (1988).
- [17] G. Blau, J. L. Coutaz, and R. Reinisch, *Opt. Lett.* **18**, 1352 (1993).
- [18] J. L. Coutaz, M. Nevriere, E. Pic, and R. Reinisch, *Phys. Rev. B* **32**, 2227 (1985).
- [19] E. V. Alieva, L. A. Kuzik, V. A. Yakovlev, G. Knippels, A. F. G. van der Meer, and G. Mattei, *Chem. Phys. Lett.* **302**, 528 (1999).
- [20] J. Heckmann, M. E. Kleemann, N. B. Grosse, and U. Woggon, *Opt. Exp.* **21**, 28856 (2013).
- [21] G. X. Li, T. Li, H. Liu, K. F. Li, S. M. Wang, S. N. Zhu, and K. W. Cheah, *Appl. Phys. Lett.* **98**, 261909 (2011).
- [22] T. Y. F. Tsang, *Opt. Lett.* **21**, 245 (1996).
- [23] J. Renger, R. Quidant, N. van Hulst, and L. Novotny, *Phys. Rev. Lett.* **104**, 046803 (2010).
- [24] P. Genevet, J. P. Tetienne, E. Gatzogiannis, R. Blanchard, M. A. Kats, M. O. Scully, and F. Capasso, *Nano Lett.* **10**, 4880 (2010).
- [25] I. Epstein, Y. Tsur, and A. Arie, *Laser Photonics Rev.* **10**, 360 (2016).
- [26] Z. Chai, X. Hu, Y. Zhu, F. Zhang, H. Yang, and Q. Gong, *Appl. Phys. Lett.* **102**, 201119 (2013).
- [27] D. Smirnova and Y. S. Kivshar, *Phys. Rev. B* **90**, 165433 (2014).
- [28] J. Guo, L. Jiang, Y. Jia, X. Dai, Y. Xing, and D. Fan, *Opt. Exp.* **25**, 5972 (2017).
- [29] M. Ishifuji, M. Mitsuishi, and T. Miyashita, *J. Am. Chem. Soc.* **131**, 4418 (2009).
- [30] R. Naraoka, H. Okawa, K. Hashimoto, and K. Kajikawa, *Opt. Commun.* **248**, 249 (2005).
- [31] *Handbook of Nonlinear Optical Crystals*, 3rd ed., edited by V. G. Dmitriev, G. G. Gurzadyan, and D. N. Nikogosyan (Springer-Verlag, Heidelberg, 1999), Chap. 4, pp. 67–288.
- [32] Y. Z. Yu, K. Y. Wong, and A. F. Garito, in *Nonlinear Optics of Organic Molecules and Polymer*, edited by H. S. Nalwa and S. Miyata (CRC Press, Boca Raton, 1996), Chap. 1, pp. 1–28.
- [33] G. T. Boyd, in *Polymers for Electronic & Photonic Application*, edited by C. P. Wong (Academic Press, Boston, 1992), Chap. 1, pp. 467–506.
- [34] L. R. Dalton, P. A. Sullivan, and D. H. Bale, *Chem. Rev.* **110**, 25 (2010).
- [35] G. Gilmour, R. A. Montgomery, S. R. Marder, L. T. Cheng, A. K. Y. Jen, C. Yongming, J. W. Perry, and L. R. Dalton, *Chem. Mater.* **6**, 1603 (1994).
- [36] H. Kan, A. Facchetti, P. Zhu, H. Jiang, Y. Yang, E. Cariati, S. Righetto, R. Ugo, C. Zuccaccia, A. Macchioni, C. L. Stern, Z. Liu, S. T. Ho, and T. J. Marks, *Angew. Chem. Int. Ed.* **44**, 7922 (2005).
- [37] Y.-J. Cheng, J. Luo, S. Hau, D. H. Bale, T.-D. Kim, Z. Shi, D. B. Lao, N. M. Tucker, Y. Tian, L. R. Dalton, P. J. Reid, and A. K.-Y. Jen, *Chem. Mater.* **19**, 1154 (2005).
- [38] T. Pliška, W. R. Cho, J. Meier, A. C. Duff, V. Ricci, A. Otomo, M. Canva, G. I. Stegeman, P. Raimond, and F. Kajzar, *J. Opt. Soc. Am. B* **17**, 1554 (2000).
- [39] A. Okada, K. Ishii, K. Mito, and K. Sasaki, *J. Appl. Phys.* **74**, 531 (1993).
- [40] Z. Sekkat, J. Wood, E. F. Aust, W. Knoll, W. Volksen, and R. D. Miller, *J. Opt. Soc. Am. B* **13**, 1713 (1996).
- [41] J. Si, J. Qiu, K. Kitaoka, and K. Hirao, *J. Appl. Phys.* **89**, 2029 (2011).
- [42] A. Sugita, Y. Sato, K. Ito, K. Murakami, Y. Tamaki, N. Mase, Y. Kawata, and S. Tasaka, *J. Phys. Chem. B* **117**, 14857 (2013).
- [43] A. Sugita, K. Ito, Y. Sato, R. Suzuki, K. Sato, T. Narumi, N. Mase, Y. Takano, T. Matsushita, S. Tasaka, and Y. Kawata, *J. Photochem. Photobio. A: Chem.* **340**, 35 (2017).
- [44] F. X. Wang, F. J. Rodríguez, W. M. Albers, R. Ahorinta, J. E. Sipe, and M. Kauranen, *Phys. Rev. B* **80**, 233402 (2009).
- [45] F. Qiu, F. Yu, A. M. Spring, and S. Yokoyama, *Opt. Lett.* **37**, 4086 (2012).
- [46] I. R. Hopper and W. L. Barnes, in *Modern Plasmonics, Maradudin*, edited by A. A. Maradudin, J. R. Sambles, and W. L. Barnes (Elsevier, Amsterdam, 2014), Chap. 2, pp. 32–74.
- [47] G. Bachelier, J. Butet, I. Russier-Antoine, C. Jonin, E. Benichou, and P. F. Brevet, *Phys. Rev. B* **82**, 235403 (2010).
- [48] C. E. Reed, J. Giergiel, J. C. Hemminger, and S. Ushioda, *Phys. Rev. B* **36**, 4990 (1987).
- [49] C. C. Katsidis and D. I. Siapkas, *Appl. Opt.* **41**, 3978 (2002).
- [50] N. Hashizume, M. Ohashi, T. Kondo, and R. Ito, *J. Opt. Soc. Am. B* **12**, 1894 (1995).
- [51] M. Born and E. Wolf, *Principle of Optics* (Cambridge University Press, Cambridge, 1999), Chap. 1, pp. 1–74.
- [52] P. B. Johnson and R. W. Christy, *Phys. Rev. B* **6**, 4370 (1972).
- [53] G. Beadie, M. Brindza, R. A. Flynn, A. Rosenberg, and J. S. Shirk, *Appl. Opt.* **54**, F139 (2015).
- [54] M. N. Polyanski, Refractive index database (2020), <https://refractiveindex.info/about>.